

Jet formation of non-spherical bubbles close to solid boundaries

Christiane Lechner^{1,2}, Max Koch², Werner Lauterborn², Robert Mettin²

¹ *Inst. of Fluid Mechanics and Heat Transfer, TU Wien, 1060 Vienna, Austria, Email: christiane.lechner@tuwien.ac.at*

² *Drittes Physikalisches Institut, Univ. Göttingen, 37077 Göttingen, Germany, Email: robert.mettin@phys.uni-goettingen.de*

Introduction

Due to their erosive power and cleaning capabilities, cavitation bubbles (expanding and) collapsing close to solid boundaries have been subject of intense investigations for several decades. Potential mechanisms of cavitation erosion are connected to the emission of shock waves and a high-speed axial liquid jet that pierces the bubble in direction of the solid. Until recently, for bubbles close to a flat solid boundary, only one type of jet was considered, which forms by involution of the bubble wall at the distal side from the solid. For laser-generated cavitation bubbles, this “standard jet” typically has a speed of the order of 100 m/s under normal ambient conditions [1]. For the case of bubbles *very* close to the solid a quite different type of jet is formed. Here, extremely thin jets with speeds of the order of 1000 m/s are ejected into the bubble as a result of the violent self-impact of annular liquid inflow at the axis of symmetry. This has been demonstrated numerically [2, 3], with experimental confirmation given in [4, 5] and later also in [6]. The fast annular inflow is “curvature induced”: around maximum extension the bubble shape reveals a region of higher curvature close to the outer rim, see Fig. 4 below. This part collapses faster than the remainder of the bubble, the latter being essentially of hemi-spherical shape. For a detailed discussion on the mechanism of fast jet formation, in particular the role of viscosity, see [2, 3].

Typically, numerical modeling of the dynamics of cavitation bubbles considers bubbles of initially spherical shape. However, realistic conditions of bubble generation, in general, involve asymmetries, as e.g. an elongated plasma shape in the case of laser-generated cavitation bubbles. Also, bubbles with non-spherical shape have been generated on purpose, as e.g. in [7]. It is therefore of interest, whether and to which extent the *initial* shape of the bubble influences jet formation, in particular the formation of fast jets. To this end, single (sub-)millimeter sized bubbles with spheroidal initial shape expanding and collapsing close to a solid boundary are investigated numerically. Jet formation is investigated as a function of the initial eccentricity and distance from the solid.

Bubble Model and Numerical Model

The bubble model consists of a bubble filled with a small amount of non-condensable gas (air) surrounded by water. The gas is taken to be ideal, undergoing adiabatic changes of state. The liquid is modeled as a compressible fluid with the Tait equation of state to allow for pressure waves and shock waves. The vapor pressure is small compared to the ambient pressure of $p_\infty = 101315$ Pa and therefore is neglected. Thermodynamic effects, mass ex-

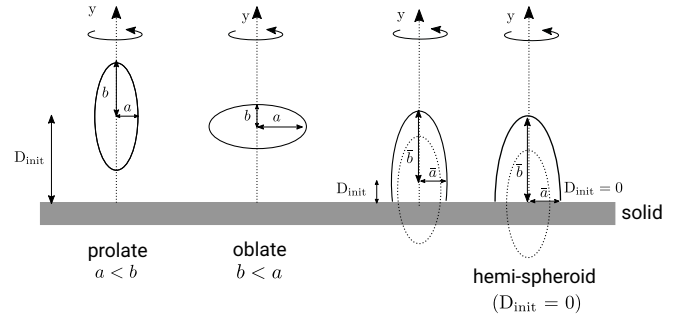


Figure 1: Sketch of the initial configuration. A bubble of initially spheroidal shape is placed at a distance D_{init} from a flat solid boundary.

change through the bubble wall as well as gravity are neglected. Liquid and gas are considered as viscous fluids. In particular, including the viscosity of the liquid is essential for fast jet formation here. Surface tension is included to comply with the simulations in [3].

Initially, a small bubble of spheroidal shape is placed at a distance D_{init} from a flat solid boundary, as sketched in Fig. 1. The initial spheroid is an ellipsoid of revolution, satisfying the equation $(x^2 + z^2)/a^2 + y^2/b^2 = 1$, where the axis of rotation (the y -axis) is taken to be orthogonal to the solid surface. This setting allows an investigation in axial symmetry. a and b denote the semi-axes of the ellipsoid. If $a < b$ the spheroid is of prolate (cigar-like) shape, if $b < a$ the shape is oblate (lentil-like), see Fig. 1 (left). For $a = b$ a sphere is obtained. The initial eccentricity can be defined as

$$e = \begin{cases} \sqrt{1 - \frac{a^2}{b^2}} & a < b, \text{ prolate,} \\ \sqrt{1 - \frac{b^2}{a^2}} & b < a, \text{ oblate,} \\ 0 & a = b, \text{ sphere.} \end{cases} \quad (1)$$

The initial volume of the bubble, V_{init} , is fixed to be equivalent to the volume of a sphere with radius $R_{\text{init}} = 20 \mu\text{m}$. Given this, the initial bubble shape is fully determined by specifying the orientation (prolate or oblate) and the eccentricity e of the spheroid.

The initial pressure in the bubble, $p_{g,\text{init}} \simeq 1.1 \times 10^9 \text{Pa}$, is chosen such that a spherical bubble in an unbounded liquid would expand to a maximum volume with $R_{\text{max}} = 500 \mu\text{m}$.

The bubbles are placed at a distance D_{init} from a plane solid boundary. If $D_{\text{init}} < b$ the spheroid would be cut by the solid surface. In this case the semi-major and semi-minor axes are re-computed to give \bar{a} and \bar{b} , such that the volume of the truncated spheroid equals V_{init} , see Fig. 1

(right). As an example, for $e = 0$ and $D_{\text{init}} = 0$ this procedure leads to a hemi-sphere with $\bar{a} = \bar{b} = 2^{1/3}R_{\text{init}}$.

R_{max} is used as the reference length in the problem, thus the dimensionless initial distance

$$D^* = D_{\text{init}}/R_{\text{max}} \quad (2)$$

is defined.

For the numerical simulations the two fluids, liquid and gas, are modeled as a single compressible medium. The Navier-Stokes equations and continuity equation are discretized with the finite volume method. The interface is captured with the volume of fluid method. We have adapted a two-phase solver from the open source software package OpenFOAM[8, 9] for our purpose [10].

Results

Spheroidal bubbles of prolate and oblate shape and eccentricities $e = 0, 0.9, 0.99$ positioned at distances $D^* \in [0, 0.3]$ from the solid are studied. For the special case of $D^* = 0$ also the more extreme values of $e = 0.995$ are included.

On a coarse scale, the *overall* dynamics of the bubbles in this parameter range is hemi-spherical to a good extent. For the case of $D^* = 0$ this is demonstrated in Fig. 2, which shows a measure for asphericity of the bubble shape as a function of time. The ratio $\zeta := x_{\text{max}}/(y_{\text{max}} - y_{\text{min}})$ of the maximum radial extension, x_{max} , over the maximum extension in direction orthogonal to the solid, $y_{\text{max}} - y_{\text{min}}$, is shown (see also Fig. 4, right column, top frame, where these quantities are indicated). For an ideal hemi-sphere $\zeta = 1$. The bubbles with $e > 0$ lose most of their initial eccentricity within the first few microseconds. For the major part of the bubble evolution ζ is close to unity. Only at the late stages of bubble evolution – before the formation of the fast jet – stronger deviations, that depend on the initial eccentricity, are observed. Bubbles with $0 < D^* \leq 0.3$ quickly almost attach to the solid at the beginning of the expansion phase. Deviations of the corresponding ζ from unity – both in magnitude of ζ and in portion of the bubble life time – increase with D^* (not shown).

The maximum volume the bubbles expand to decreases with increasing D^* and with increasing eccentricity (not shown). However, variations in the maximum equivalent radius $R_{\text{max}}^{\text{eq}} := (3V_{\text{max}}/(4\pi))^{1/3}$ are small: $R_{\text{max}}^{\text{eq}}$ varies less than 5% in the D^* interval considered and less than 2% with eccentricity. The time from generation of the bubble (corresponding to $t = 0 \mu\text{s}$ in the numerical simulations) and the first collapse, $t(V_{\text{min}})$, is very close to twice the Rayleigh collapse time, T_c , of a sphere with radius $2^{1/3}R_{\text{max}}^{\text{eq}} \simeq 1.26R_{\text{max}}^{\text{eq}}$. This relation reflects the predominantly hemi-spherical collapse. The numerical simulations give

$$t(V_{\text{min}}) \simeq 2 \times \underbrace{1.28 \times 0.915 \times R_{\text{max}}^{\text{eq}}}_{T_c(1.28 \times R_{\text{max}}^{\text{eq}})} \times \sqrt{\rho_{\infty}/p_{\infty}}, \quad (3)$$

as shown in Fig. 3, for the whole parameter range under consideration. The pre-factor 1.28 instead of 1.26 might be attributed to the non-condensable gas in the bubble.

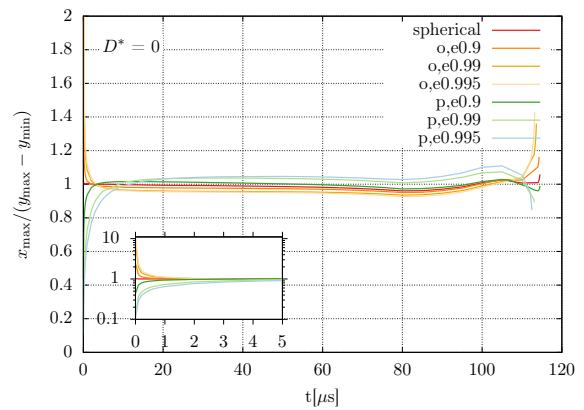


Figure 2: Asphericity, $x_{\text{max}}/(y_{\text{max}} - y_{\text{min}})$, as a function of time for bubbles expanding and collapsing right at the solid surface, $D^* = 0$. The evolution is shown up to the formation of the fast jet. The insert shows a zoom into the first few microseconds of bubble evolution. The initial bubble shapes are spherical as well as oblate (“o”) and prolate (“p”) spheroids with eccentricity “exx”.

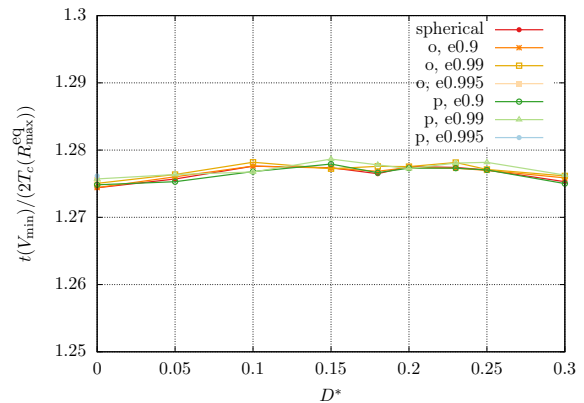


Figure 3: Time from generation of the bubble to the first collapse $t(V_{\text{min}})$ as a function of D^* . $T_c(R_{\text{max}}^{\text{eq}})$ denotes the Rayleigh collapse time of a spherical bubble with radius $R_{\text{max}}^{\text{eq}}$.

A closer inspection of the bubble shapes, in particular during the collapse phase, reveals important and striking deviations from hemi-spherical shape. Fig. 4 shows the bubble shapes for the case $D^* = 0$ at three special moments of bubble evolution, namely close to the moment of maximum extension (top row), shortly before the formation of the fast jet (middle row) and shortly after the formation of the fast jet (bottom row). Around maximum extension the bubble shape reveals a small gap between the outer rim of the bubble and the solid. This can be attributed to the action of viscosity during the rapid expansion of the bubble. Although this deviation from hemi-spherical shape might seem marginal for bubbles in water, it is decisive for the fast jet forming in the late collapse phase. The high curvature region at the outer rim collapses faster than the remainder of the bubble leading to an indentation and the typical bell shape of the collapsing bubble (not shown here), that first has been photographically presented in [11]. In the middle row of Fig. 4 the bubble shape is captured at a moment shortly before the high speed annular inflow (showing as

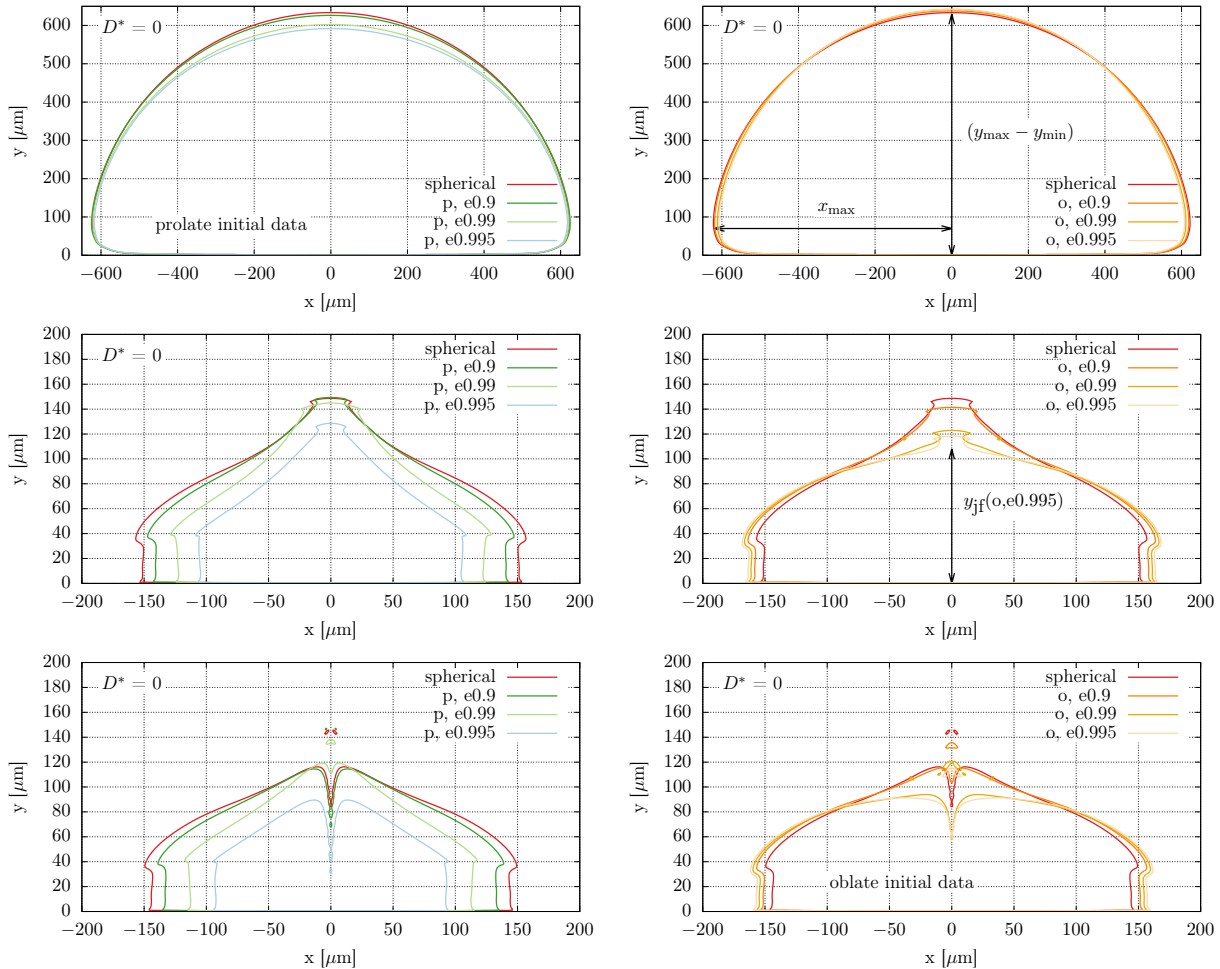


Figure 4: Bubbles generated right at the solid boundary, $D^* = 0$. The initial shapes of the bubbles are hemi-spheroids (prolate, “p”, left column and oblate, “o”, right column) with given eccentricity e . Shown is the bubble shape (a cut through the bubble) at maximum extension (top row), shortly before the formation of a fast jet (middle row) and shortly after the formation of a fast jet (bottom row). The time intervals between middle row and bottom row are $0.1 \mu\text{s}$. The parameters x_{max} and $y_{\text{max}} - y_{\text{min}}$ for measuring asphericity are indicated in the top frame of the right column. The definition of y_{jf} – the distance of the point of self impact at the axis from the solid – is indicated in the middle frame of the right column for the initially oblate spheroid with $e = 0.995$.

an indentation) impacts onto itself at the axis. The next row shows the bubble shapes only 100 ns later, with the fast jet rushing through the bubble towards the solid. The middle and last rows show clear deviations in shape among the bubbles with different initial shape.

The speed of the fast jet – as obtained from simulations on a computational grid with a minimum grid spacing of $1 \mu\text{m}$ – is given in Fig. 5 as a function of D^* . Note, that fast jet formation is a nearly singular phenomenon. Correspondingly, grid convergence of the jet speed could not be obtained in axial symmetry [3]. Nevertheless, the figure might indicate the trend in variations of the jet speed. The speed of the fast jet is of the order of 1000 m/s and shows strong variations both with D^* and with the orientation and eccentricity of the initial spheroid. An initial oblate shape tends to result in a smaller jet speed, while an initial prolate shape with sufficient eccentricity

leads to larger jet speeds for $D^* \gtrsim 0.1$. The insert in Fig. 5 gives the values for the standard jet for $0.23 \lesssim D^* \leq 0.3$, the standard jet being more than one order of magnitude slower than the fast jet. Deviations of up to $\pm 20\%$ in the jet speed are observed when varying the initial shape of the bubble.

Discussion and Outlook

The dynamics of bubbles of initially spheroidal shape has been investigated numerically for a range of initial distances $D^* \in [0, 0.3]$. The bubbles quickly loose most of their eccentricity (up to even slightly “reversing” the orientation, see Fig. 2). This might be attributed to a kind of “flow de-focusing”: more strongly curved parts of the bubble surface expand slower than less curved parts (for a discussion of “flow focusing” for collapsing bubbles see [3, Appendix C]).

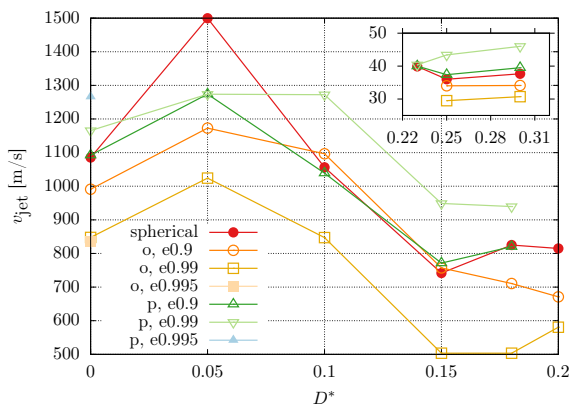


Figure 5: Jet speed as a function of D^* as obtained from simulations on a computational grid with a minimum grid spacing of $1\ \mu\text{m}$. The main frame shows the speed of the fast jet for $D^* \lesssim 0.2$, the insert shows the speed of the standard jet for D^* values $\gtrsim 0.23$. Note the different scales on the y -axes.

Bubbles in the considered parameter range show a collapse time that differs from the Rayleigh collapse time by a uniform factor of 1.28 in our model. This relation is of interest, e.g., for laser generated bubbles: information on the maximum extension of the bubble ($R_{\text{max}}^{\text{eq}}$) can be drawn from measuring the time difference between the shock wave emitted at bubble generation and the shock wave emitted upon the first collapse of the bubble via Eq. (3).

It has been shown, that fast jet formation is a robust phenomenon with respect to initial shape deformations. The transition from fast jet formation to standard jet formation when varying D^* is complex, as described in [3] for initially spherical bubbles. The initial bubble shape has a small influence on the D^* values of the transition region as well as on the precise phenomena at the transition (not shown here).

For fixed D^* , characteristic quantities of both types of jets (“fast” and “standard”) visibly are influenced by the initial shape of the bubble. In particular, the speed of the jet, v_{jet} , varies by up to 20% with the initial eccentricity. For $D^* \lesssim 0.2$ and the formation of fast jets there is a tendency that the jet speed increases from initially oblate bubbles with high eccentricity over initially spherical bubbles to initially prolate bubbles with high eccentricity. Further investigations are necessary, to see whether this trend can be related directly to curvatures of the bubble shape at maximum extension (see Fig. 4). For the speed of the standard jet for $D^* \gtrsim 0.23$ this ordering in jet speeds is unambiguous (oblate with $e = 0.99$ leading to the lowest, prolate with $e = 0.99$ leading to the highest jet speed). The influence of initial eccentricity on the jet speed for larger D^* values will be subject of further research.

Acknowledgments

The work was supported in part by the German Science Foundation (DFG) under contracts Me 1645/8-1 and Me 1645/8-3 and the Austrian Science Fund (FWF) (Grant

No. I 5349-N).

References

- [1] Philipp, A. and Lauterborn, W.: Cavitation erosion by single laser-produced bubbles. *Journal of Fluid Mechanics* 361 (1998), 75–116
- [2] Lechner, C., Lauterborn, W., Koch, M. and Mettin, R.: Fast, thin jets from bubbles expanding and collapsing in extreme vicinity to a solid boundary: A numerical study. *Physical Review Fluids* 4 (2019), 021601
- [3] Lechner, C., Lauterborn, W., Koch, M. and Mettin, R.: Jet formation from bubbles near a solid boundary in a compressible liquid: Numerical study of distance dependence. *Physical Review Fluids* 5 (2020), 093604
- [4] Koch, M.: Laser cavitation bubbles at objects: Merging numerical and experimental methods. PhD thesis, Georg-August-Universität Göttingen, Third Physical Institute (2020). <http://hdl.handle.net/21.11130/00-1735-0000-0005-1516-B>
- [5] Koch, M., Rosselló, J. M., Lechner, C., Lauterborn, W., Eisener, J. and Mettin, R.: Theory-assisted optical ray tracing to extract cavitation-bubble shapes from experiment. *Experiments in Fluids* 62 (2021), 60
- [6] Reuter, F. and Ohl, C.-D.: Supersonic needle-jet generation with single cavitation bubbles. *Applied Physics Letters* 118 (2021), 134103
- [7] Lim, K. Y., Quinto-Su, P. A., Klaseboer, E., Khoo, B. C., Venugopalan, V. and Ohl, C.-D.: Nonspherical laser-induced cavitation bubbles. *Physical Review E* 81 (2010), 016308
- [8] Weller, H. G., Tabor, G., Jasak, H. and Fureby, C.: A tensorial approach to computational continuum mechanics using object-oriented techniques. *Computers in Physics* 12 (1998), 620–631
- [9] The foam-extend project, URL: <https://sourceforge.net/projects/foam-extend/>
- [10] Koch, M., Lechner, C., Reuter, F., Köhler, K., Mettin, R. and Lauterborn, W.: Numerical modeling of laser generated cavitation bubbles with the finite volume and volume of fluid method, using OpenFOAM. *Computers & Fluids* 126 (2016), 71–90
- [11] Benjamin, T. B. and Ellis, A. T.: The collapse of cavitation bubbles and the pressures thereby produced against solid boundaries. *Philosophical Transactions of the Royal Society of London, Series A: Mathematical, Physical and Engineering Sciences* 260 (1966), 221–240